Dual-User Massive MIMO Measurements at 3.5GHz with Bi-Directional Angular Discrimination

Karstensen, Anders; Nielsen, Jesper Ødum; Eggers, Patrick Claus F.; Carvalho, Elisabeth De; Alm, Martin; Steinbock, Gerhard

Published in:
12th European Conference on Antennas and Propagation (EuCAP)

DOI (link to publication from Publisher):
10.1049/cp.2018.0728

Publication date:
2018

Document Version
Accepted author manuscript, peer reviewed version

Dual-User Massive MIMO Measurements at 3.5GHz with Bi-Directional Angular Discrimination

Anders Karstensen[1], Jesper Ø. Nielsen[1], Patrick Eggers[1], Elisabeth De Carvalho[1],
Martin Alm[2], Gerhard Steinböck[2]
[1]Antennas, Propagation and Millimetre-wave Systems, Department of Electronic Systems, Aalborg University, Denmark
[2]Huawei Technologies Sweden AB

***Abstract*—This paper presents a Massive-MIMO measurement campaign with bi-directional angular discrimination. Aspects like non-stationarity, spatial consistency and spherical wavefronts become important for proper modeling of such channels. This campaign is designed to measure and investigate these aspects of the channel. The paper includes analyses of the angular statistics and the dual directional power angular spectrum for a few locations. Next, the paths/clusters are mapped to a 2D map for visualisation of clusters. Finally, non-stationarity across the large array aperture is investigated in terms of angular statistics and power.**

***Index Terms*—Massive-MIMO, Dual user, propagation, measurement.**

I. Introduction

Massive MIMO has gained a lot of interest in recent years, and is considered to be one of the key technologies in the next generation wireless communication systems [1]. To simulate and model the massive MIMO channel, several challenges arise when trying to incorporate them into existing geometry-based stochastic channel models (GSCM). The work presented in [2] and [3] proposes an extension of the COST 2100 model and the QuaDRiGa model, respectively. Both papers mention three features of massive MIMO that need to be included to properly simulate massive MIMO systems. The models should include methods of modeling; multiuser consistency, non-stationarity across the base station array and spherical wavefronts. These features are reported in previous measurement campaigns [4], [5] and require further investigation. This paper presents a large measurement campaign in an indoor stadium, with multiple routes designed to investigate these features for calibration and further extensions of massive MIMO compatible models.

Section II will introduce the measurement system and location. An analysis of the angular properties of the measured channel is detailed in Section III. Section IV will analyse the location and commonality of clusters based on a visual mapping of scatter locations. Section V will analyse the non-stationarity across the massive 128 element array, and section VI concludes this paper.

II. Measurement Setup

The measurement campaign was conducted in Gigantium in Aalborg, which houses a large indoor stadium. It is a typical handball field of 20x40 m, with large tribune sections surrounding the field in all directions. The tribune section is about 65x72 m. A drawing of the stadium is depicted in Fig. 1, where the position of the RX array along with a few measurement routes indicated. The map shows roughly half of the large hall, the remaining area is mostly empty space, and situated to the right of the stadium shown in Fig. 1.

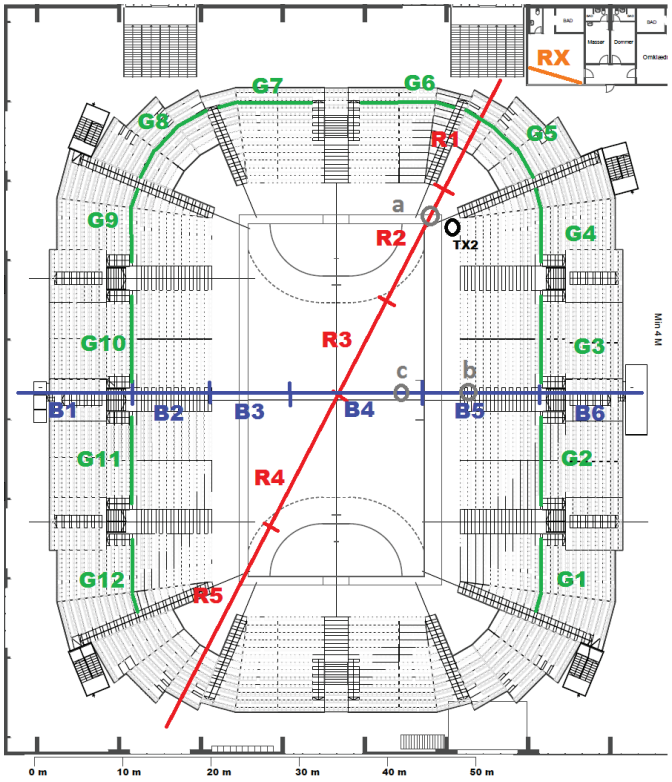

Fig. 1: Measurement map, Tx routes and location of the massive Rx array.

A. Array configuration

The massive Rx (Receiver) array is configured as a Uniform Linear Array (ULA) consisting of 128 Vivaldi horn elements [6]. The half power beamwidth of the Vivaldi elements are about 44 degrees in azimuth, and 49 degrees in elevation. For practical reasons, the elements are grouped in modules of 16 elements. The element spacing is 5 cm, or 0.58 λ at 3.5 GHz,

(a) 128 element massive MIMO receiver array

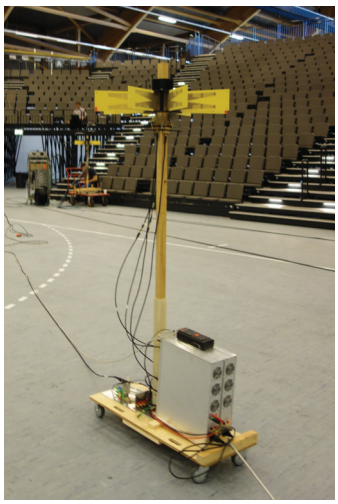

(b) Mobile Circular transmitter array, Tx1

giving a total array length of 6.35 meters. The array is depicted in Fig. 2a.

Two Tx (transmitter) arrays are configured as Uniform Circular Arrays (UCA) consisting of 8 Vivaldi horn elements each. The radius to the phase center at 3.5 GHz is about 22 cm, which is unfortunately too large for any phased array processing but was required for mechanical reasons. The Tx-array denoted as Tx2 is connected to the Tx-rack directly by short rf-cables. The Tx-array denoted as Tx1 is much more mobile and independent of the Tx-rack. This is accomplished by moving the rf amplifiers onto the "trolley" carrying the array. RF to fiber optical interfaces and cables connect the Tx rack to the amplifiers on the trolley. During this measurement campaign we were limited to only 4 optical amplifiers, meaning the mobile Tx1-array only has 4 channels. Two neighbouring elements in this array are combined to reduce the 8 elements to 4. Thus the 4 channels cover all azimuth directions. Tx1 is clearly depicted in the foreground in Fig. 2b and Tx2 is visible in the background.

B. Measurement equipment

The Massive-MIMO measurement system is based on the correlation based AAU channel sounder [7]. A carrier frequency of 3.5 GHz and a bandwith of 100 MHz was used. The sounder has 16 fully parallel transmitters and 8 fully parallel receivers. A fast switching mechanism on the Rx modules allows the sounder to capture a snapshot of the 128x16 MIMO channel in 1.31 ms. For each measurement, 900 snapshots of the channel is recorded during 15 seconds correspondent to a snapshot rate of 60 Hz.

The Tx rack is synced to the Rx rack by a fiber optical cable, allowing a Tx-Rx separation of about 300 m. As mentioned in Sec. II. A, Tx1 is separated via fiber optical cables (300m length) from the Tx-rack. Thus the maximum possible distance between Rx and Tx1 is approximately 600m. Tx2 is connected by RF cables and thus can only be in the proximity of the Tx-rack with an approximate maximum Rx to Tx2 distance of 300m.

C. Measurement scenarios

The measurements consist mainly of one semi-stationary Tx array, while the other one is moving along a route in the stadium. Three large routes of Tx1 are depicted in Fig. 1 by the lines, denoted as R, G and B, respectively. A route is typically separated into smaller sections as each measurement is only 15 seconds long. Walking for instance the full diagonal (red) of the field is split into 5 sections of 15 second measurements to cover the full distance. During the measurements, when Tx1 is moving along these routes, Tx2 is being rocked back and fourth +/- 10 cm. The Tx2 location is marked by the black circle "TX2" in Fig. 1.

III. Angular analysis

In this analysis a beam-scanning was performed from the RX array to each individual Tx element. The Tx element separation is too large for array processing techniques. Thus each element represents the respective 45/90 degree sections. The angular analysis is initially restricted to 2 modules (32 elements) of the Rx array to avoid possible errors due to non-stationarity across the large array.

The Direction Of Arrival (DOA) estimation is performed according to the Bartlett beamformer:

$$DOA(\theta, \theta_{tx}) = a^*(\theta)\hat{R}a(\theta) \tag{1}$$

where θ is discrete with a 1 degree resolution, and θ_{tx} is discrete with 45/90 degree resolution. $()^*$ denotes the complex conjugate transpose and:

$$a(\theta) = [1\ e^{-i\omega s} ...\ e^{-i(m-1)\omega s}]^T \cdot P_{ant}(\theta) \tag{2}$$

where $()^T$ denotes the Transpose operator, m is the antenna number and the spatial frequency ωs:

$$\omega s = \frac{2\pi}{\lambda} d \sin(\theta) \tag{3}$$

Each vector $a(\theta)$ is multiplied by the normalized antenna element pattern gain $P_{ant}(\theta)$. A Hamming window of size M is also applied to the vector $a(\theta)$.

In (1), $\hat{R}$ is the estimated covariance matrix given by:

$$\hat{R} = \frac{1}{N} \sum_{t=1}^{N} y(t) y^*(t) \tag{4}$$

where $y(t)$ is a vector of the narrowband time domain signal of all Rx antennas at snapshot time t. N is the number of snapshots included in the estimation.

The Power angular spectrum seen from Tx or Rx array is given by:

$$PAS(\theta) = \sum_{\theta_{tx}} DOA(\theta, \theta_{tx}) \tag{5}$$

$$PAS(\theta_{tx}) = \sum_{\theta} DOA(\theta, \theta_{tx}) \tag{6}$$

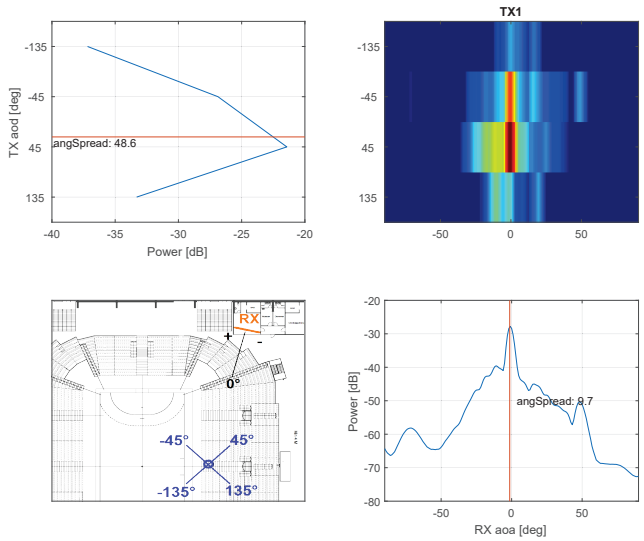

Fig. 3: Tx1 Dual directional and PAS for location "b" indicated in Fig. 1.

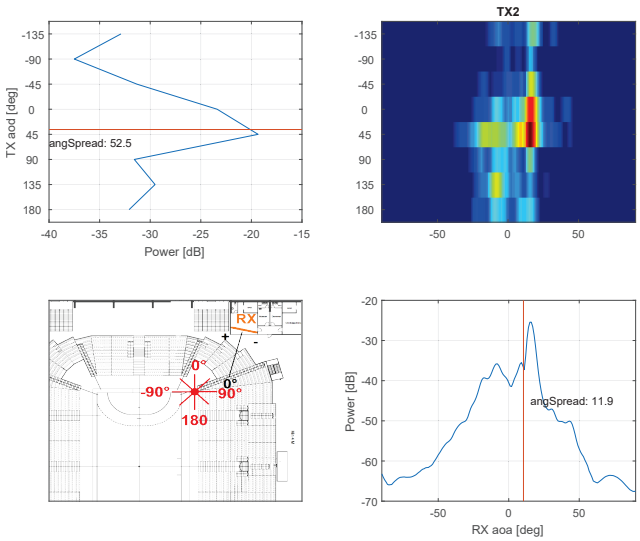

Fig. 4: Tx2 dual directional and PAS for location "TX2" indicated in Fig. 1.

Mean azimuth angle μ_θ and azimuth angle spread σ_θ can be calculated, as defined in [8], to account for the ambiguity of the modulo 2π operation:

$$\sigma_\theta = \min_{\Delta} \sigma_\theta(\Delta) = \sqrt{\frac{\sum_i (\theta_{i,\mu}(\Delta))^2 \cdot P_i}{\sum_i P_i}} \tag{7}$$

where P_i is the power at the i-th direction and $\theta_{i,\mu}(\Delta)$ is defined as

$$\theta_{i,\mu}(\Delta) = mod(\theta_i(\Delta) - \mu_\theta(\Delta) + \pi, 2\pi) - \pi \tag{8}$$

The mean angle is defined as

$$\mu_\theta(\Delta) = \frac{\sum_i \theta_i(\Delta) \cdot \sum_\tau P_i}{\sum_i P_i} \tag{9}$$

and $\theta_i(\Delta) = mod(\theta_i + \Delta + \pi, 2\pi) - \pi$

Figures 3 and 4 top right show the narrowband beamforming results from the Rx array to the individual elements in the two Tx arrays. Top left figure shows the Power Angular Spectrum (PAS) from the Tx array where as the bottom right shows the PAS from the Rx array. The bottom left figure indicates the respective location and element(combined elements) orientation of the Tx arrays. The red line indicates the mean angle of the respective PAS. In Fig. 3 bottom right figure we see the the mean angle coincides almost at broadside of the array for the chosen location of Tx1.

In Fig. 5 and 6 the angular spread and mean are plotted for the entire section B5 of route B indicated in Fig. 1. Each point is an average over 100 snapshots, and the length of section B5 is about 13 meters. In Fig. 5 we see as expected, that the mean angle towards Tx1 changes as it moves up the stairs of the tribune, while Tx2 does not change as it is stationary. Seen from the Tx side in Fig. 6, we see the same trends for mean

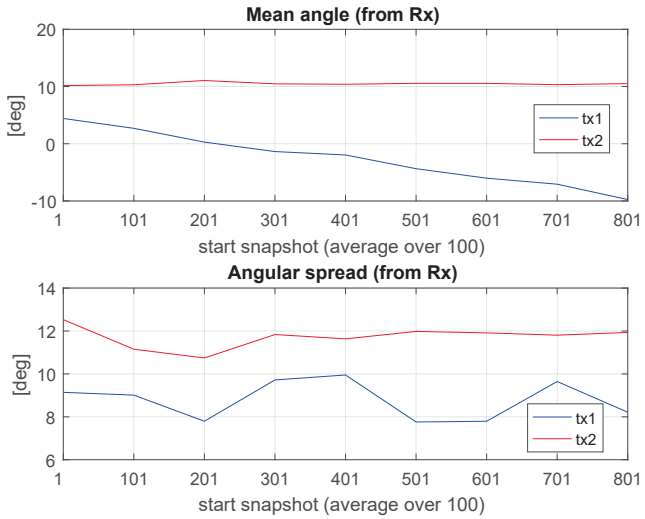

Fig. 5: Mean and spread from Rx array.

angle, but with large variations while walking along the route. This is not unexpected as the angular resolution is very low at the Tx side, and it is difficult to maintain a fixed orientation of the array while it is carried up the stairs of the tribune. The angular spread is much larger at the Tx side compared to the Rx side. The angular spread does not vary with any notable trend from any of the Tx's in Fig. 5 and 6.

In Fig. 7 the PAS from Rx to the two Tx arrays for section B5 is shown with the same averaging and intervals as in Fig. 5 and 6. The movement of Tx1 is clearly visible from this plot.

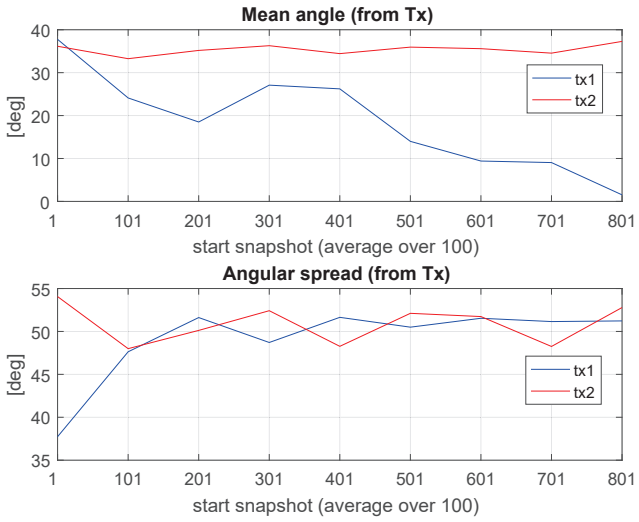

Fig. 6: Mean and spread from Tx array.

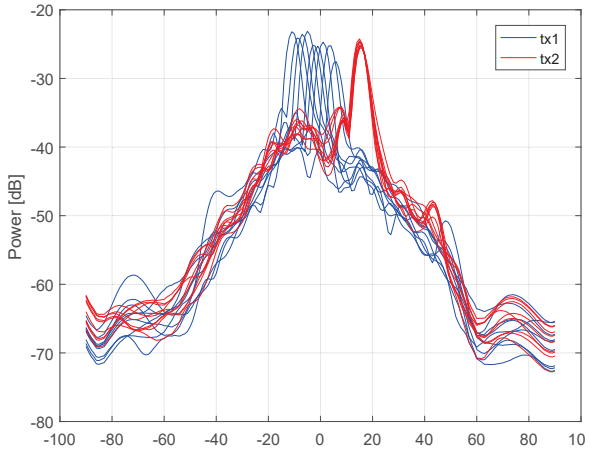

Fig. 7: PAS from Rx towards Tx1 and Tx2 for the 9 parts of section B5 in Fig. 1.

IV. Cluster visualisation

This section describes the mapping of scattering points on to a 2D map with respect to the Rx and Tx locations. The paths are selected from the wideband angular-delay profiles, which are obtained by performing the beamforming in (1) at each measured delay tap.

The scatter points are all assumed to be single bounce scatterers. Given the position of Rx and Tx array and the delay and AoA of the path in question, the position of the scatterer is estimated by simple geometric triangle calculations. In Fig. 8 the Rx and Tx array locations are plotted, and the estimated scattering points are indicated too by red and blue solid circles. Larger circles indicate more power of the path in question. As seen in Fig. 8, Tx1 and Tx2 are separated by about 2.5 m. The large clusters formed by closely spaced scattering points are overlapping, meaning there is typically scattering points from both Tx arrays in the same area.

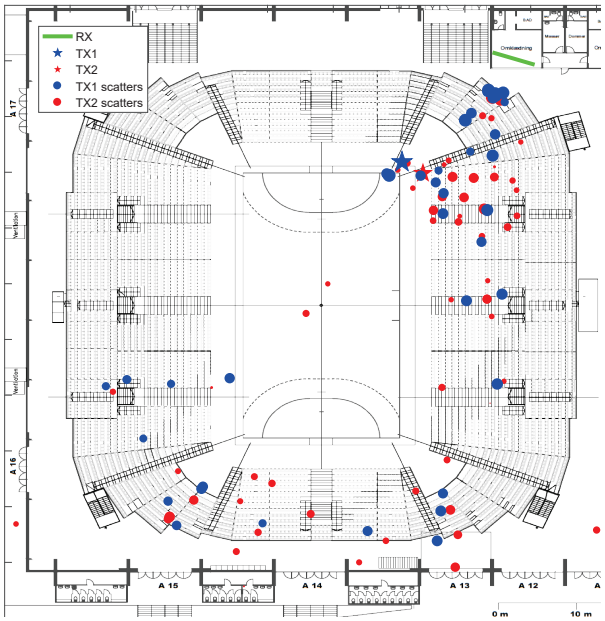

Fig. 8: Mapped scattering points, closely separated Tx's. Location "a" and "TX2" in Fig. 1.

In Fig. 9, Tx1 has moved further down the diagonal and is now positioned in the center of the arena. The two Tx's are now separated by a larger distance, ie. approximately 23 m. The two Tx's are still in a similar direction as seen from the Rx array. Comparing with Fig. 8, the majority of Tx1 scatterers are now in the bottom-left end of the arena, while the majority of Tx2 scatterers are still in the top-right end of the arena. Separating larger areas into cluster that are either blue or red dominant is now much easier as compared to the case of closely spaced Tx arrays. This user separation and the resulting overlapping/non-overlapping should be considered in propagation models.

V. Non-stationarity

This section will take a look at the non-stationarity from the perspective of the large receiver array aperture.

In Fig. 10 the mean and angular spread is calculated independently for each of the 8 modules in the massive receiver array. The mean and spread is calculated from spatial averaging over 20 and 100 snapshots, corresponding to 0.3 and 1.6 meter movement of Tx1. Each module contains; as previously mentioned, 16 elements. Point "c" and "Tx2" from Fig. 1 indicate the fixed positions of Tx arrays in this analysis.

As seen in Fig. 10, for the 100 snapshots mean angle, there is 8.8 and 10.3 degree change from the first module to the last. The geometrical difference is calculated to be 7.8 and 11.7 degree. The maximum difference in angular spread over the array is about 6-10 degrees.

In Fig. 11 the average power over 100 snapshots is plotted for every Rx-Tx element pair. Except for minor differences, the same overall result was obtained for the average power over 20 snapshots.

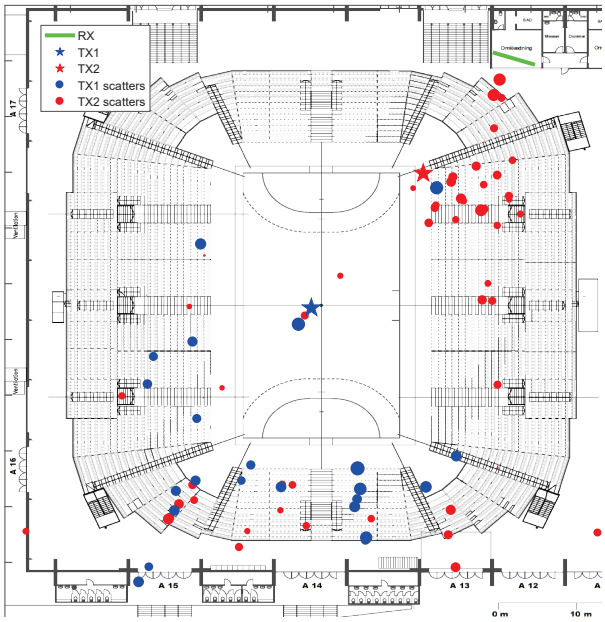

Fig. 9: Mapped scattering points, largely separated Tx's.

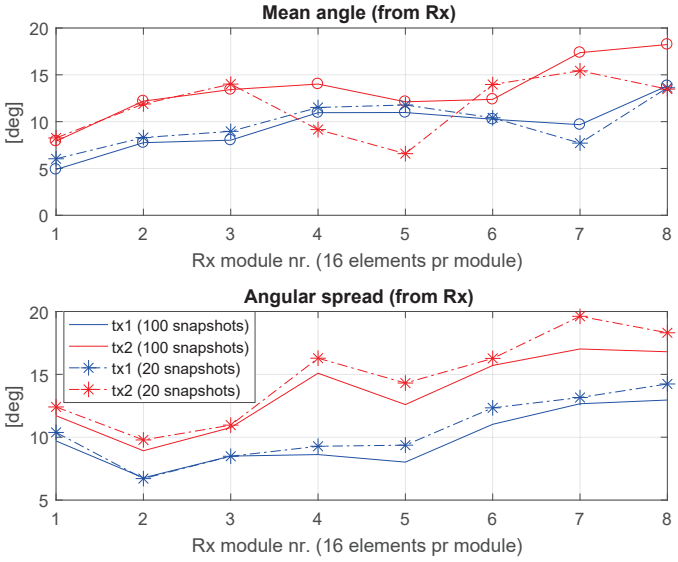

Fig. 10: Angular mean and spread per module (16 elements) of the massive receiver array.

There are large variations in power across the array, most notably for the Tx elements with high power. The figure shows typically more power in the left side of the Rx array. These effects should be studied further and should be considered in modelling of massive MIMO channels.

VI. Conclusion

In this paper we have studied the average power-angular properties of a dual user massive MIMO measurement campaign set in an indoor stadium scenario. From the examples in the angular analyses, angular spread is much larger around the mobile station compared to the base station. When visualizing clusters on the map of the arena, we showed an increase in cluster overlapping with decreasing user separation. Lastly, non-stationarity across the large array aperture was demonstrated in terms of power variations and changes in angular mean and spread.

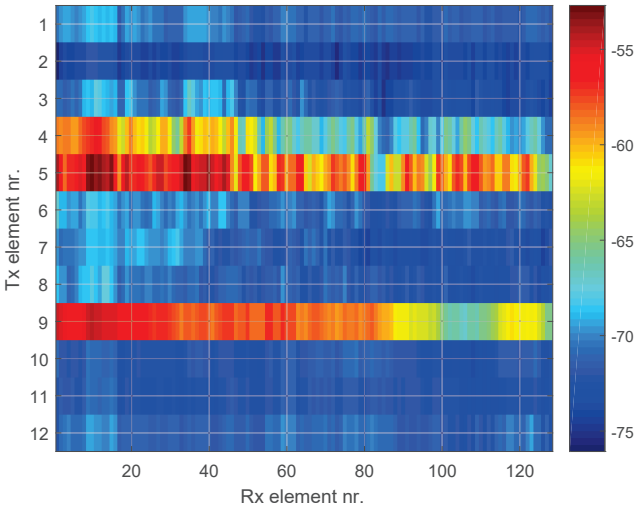

Fig. 11: Mean power for all Tx-Rx element pairs. Elements 1-8 belongs to Tx2, and elements 9-12 belongs to Tx1.

Acknowledgment

The authors would like to thank Huawei Sweden AB for their financial support.

References

[1] E. G. Larsson, O. Edfors, F. Tufvesson, and T. L. Marzetta, "Massive MIMO for next generation wireless systems," *IEEE Communications Magazine*, vol. 52, no. 2, pp. 186–195, February 2014.

[2] X. Gao, J. Flordelis, G. Dahman, F. Tufvesson, and O. Edfors, "Massive mimo channel modeling - extension of the cost 2100 model," 2015.

[3] À. O. Martínez, P. Eggers, and E. D. Carvalho, "Geometry-based stochastic channel models for 5G: Extending key features for massive MIMO," in *2016 IEEE 27th Annual International Symposium on Personal, Indoor, and Mobile Radio Communications (PIMRC)*, Sept 2016, pp. 1–6.

[4] À. O. Martínez, E. D. Carvalho, and J. . Nielsen, "Towards very large aperture massive MIMO: A measurement based study," in *2014 IEEE Globecom Workshops (GC Wkshps)*, Dec 2014, pp. 281–286.

[5] S. Payami and F. Tufvesson, "Channel measurements and analysis for very large array systems at 2.6 ghz," in *2012 6th European Conference on Antennas and Propagation (EUCAP)*, March 2012, pp. 433–437.

[6] S. Zhang, T. L. Jensen, O. Franek, P. C. F. Eggers, C. Byskov, and G. F. Pedersen, "Investigation of a UWB wind turbine blade deflection sensing system with a tip antenna inside a blade," *IEEE Sensors Journal*, vol. 16, no. 22, pp. 7892–7902, Nov 2016.

[7] J. O. Nielsen, J. B. Andersen, P. C. F. Eggers, G. F. Pedersen, K. Olesen, and H. Suda, "Measurements of indoor 16 times;32 wideband MIMO channels at 5.8 GHz," in *Eighth IEEE International Symposium on Spread Spectrum Techniques and Applications - Programme and Book of Abstracts (IEEE Cat. No.04TH8738)*, Aug 2004, pp. 864–868.

[8] 3GPP TR 25.996, "Spatial channel model for multiple input multiple output (MIMO) simulations," Tech. Rep., march 2017.